Modeling the Functional Organization of the Visual Cortex

L. Sirovich, R. Everson, E. Kaplan, B.W. Knight, E. O'Brien and D. Orbach

Laboratory of Biophysics,
Rockefeller University, NYC 10021
Laboratory of Applied Mathematics
Mt. Sinai Medical School and CUNY, NYC 10029

While many models of the dynamics and interactions of single neurons are extant, analogous constructs which attempt to describe large-scale ($\geq O\ (10^8)$) neuronal activity are few and far between. Optical imaging of the visual cortex makes such macroscopic neuronal activity accessible. Symmetries latent in the cortical architecture are used here to develop a scheme for analyzing such images. In this way, intrinsic modes of cortical response can be uncovered, using minimal assumptions. Some of these modes correspond to already-familiar features of the functional architecture, and it is highly likely that others hold physiological relevance as well. Finally, the number of such modes that would be required in a more fully developed model (incorporating cortical dynamics) is approximated.

Key words: dynamics, visual cortex, eigenfunctions, symmetry, ocularity, orientation

[1] Supported by NIMH R01MH50166-01, ONR N00014-95-1-0281 & N00014-93-1-0279.

1 Introduction

The dynamics of a single neuron may be regarded as a well understood problem. Hodgkin-Huxley theory (see e.g. [1]) provides both a solution to the problem and a framework for further refinement of single neuron dynamics. However well understood this may be, when confronted by the interaction of the $O(10^{10})$ neurons that compose the mammalian brain, one is reminded of the insignificant role of the dynamics of single molecules in the macroscopic description of the flow of a gas. Several computational models of the cortex have been based on the interaction of populations of individual neurons ([2], [3]), but thus far only a few dynamical macroscopic (mathematical) models of the brain or parts of it have been advanced. In this investigation we consider the mammalian visual cortex, with the eventual goal of constructing a model of large scale interacting populations of neurons, participating in macroscopic modalities such as eye preference (ocularity), orientation preference, color, texture and so forth.

Evidence for the existence of coherent macroscopic organization is available from experiment, especially for the visual cortex. For example Hubel & Wiesel [4], [5] showed that primary visual cortex is parceled into vertical columns of neurons coded for like orientations, with nearby columns coded for nearby orientations. Individual cells appear to be binocular, but generally, stimulation of one eye dominates over the other. Staining procedures have demonstrated that patterns of ocular dominance appear in segregated stripes that meander and bifurcate in a rich and somewhat chaotic pattern [6]. Visual modalities must find in the cortex locations where they are represented. It is thus reasonable to find that in the visual cortex of cat or monkey, orientation columns reside within the ocular dominance columns: each region of eye preference contains a population of neurons which respond to the full range of orientations. The same theme, namely that macroscopic assemblies of neurons of the cortex are engaged in like activity, also emerges from imaging of cortical activity [7–11]. This approach provides the central impetuous for the deliberations of the present paper.

At the level of the primary visual cortex the transmitted visual information has already undergone a number of transformations or mappings. The cortical map is a topographic (continuous) map of retinal areas of responsiveness, known as receptive fields. The modalities of orientation and ocular dominance play a central role in the cortical map. Starting with the *ice cube* model [12] and the *pinwheel* model [13,14] a range of models has been proposed for orientation and ocular dominance and a critical comparative study of the many ensuing models has recently appeared [15]. The investigation which follows is different in spirit from these studies, in that no model is proposed. Rather, we explore the consequences (applicable to *any* such model) of latent symmetries

present in the cortical architecture and hence in the response images that are generated from it. The symmetries provide organizing principles for analyzing and viewing the data.

2 Background

Visual space is divided by the mammalian visual system into right and left hemifields. Each hemifield is projected to the contra-lateral visual cortex. Thus the normal right and left visual cortices each receive inputs from both the contra-and ipsi-lateral eyes, in essentially equal proportion. Stimulation of the visual system may be performed either monocularly or binocularly. In exploring cortical response a rich variety of visual stimuli, $S(t)$, are introduced in order to elicit the various modalities that vision appears to encompass.

In the following we will denote cortical response by

$$\phi = \phi(t, \mathbf{x}) \tag{1}$$

where ϕ, the recorded "gray level" measures neural activity at pixel location $\mathbf{x}$ at time t. (It will not be necessary to distinguish between continuous and discrete variables.) We shall also use ϕ to denote the time history of cortical images collected in an experiment; a component of this signal is a result of neural activity. The so-called "intrinsic signal" measures the reflectance of light from the tissue induced by local changes due to neural activity [10], while fluorescence signals from appropriate dyes directly measure voltage changes [16,17].

In order to make explicit the dependence of ϕ on the stimulus, we can also write (1) as,

$$\phi = \phi(t, \mathbf{x};\, S[t']). \tag{2}$$

The form $S[t']$ is intended to convey the concept that the response ϕ, at $(t, \mathbf{x})$ is a functional that depends on the entire past history $t' \leq t$ of the stimulus, S.

Although a dynamical theory of the cortex is an eventual goal, in the work we present here transient effects will be regarded as having been averaged out (functional architecture rather than dynamics is being considered at this stage). Thus, instead of (2) we will consider

$$\phi = \phi(S(t), \mathbf{x}) \tag{3}$$

so that t plays the role of an index for the presented stimulus and ϕ is the appropriately averaged image elicited in response to the stimulus. In effect the function $S(t)$ provides a lookup table from which we find the stimulus presented at time t. Although we will continue to use (1) it should be regarded as shorthand for (3). Also on the notational side, when appropriate we will replace $S(t)$ in (3) by a vector which more explicitly indicates the nature of the stimulus. For example, a spatial pattern that is frequently used as a visual stimulus is a repeated array of drifting parallel bars oriented at some reference angle θ. In this case we will write,

$$\phi = \phi(e(t), \theta(t), x), \tag{4}$$

for the image captured in response to the stimulation of the left or right eye, $e(t)$,with a pattern which has orientation $\theta(t)$.

3 Data Analysis

In order to characterize cortical images we introduce sufficiently complete sets of orthonormal functions, to be defined below, in time $\{a_n(t)\}$ and in space $\{\psi_n(\mathbf{x})\}$, *i.e.,*

$$(a_n, a_m)_t = \sum_t a_n(t) a_m(t) = \delta_{mn}, \tag{5}$$

and

$$(\psi_n, \psi_m)_{\mathbf{x}} = \sum_{\mathbf{x}} \psi_n(\mathbf{x}) \psi_m(\mathbf{x}) = \delta_{mn}, \tag{6}$$

and constants $\{\mu_n\}$ so that we may write

$$\phi(t, \mathbf{x}) = \sum_n a_n(t) \mu_n \psi_n(\mathbf{x}). \tag{7}$$

(In (5) and (6) and in the following $\sum$ is shorthand for either discrete summation or continuous integration.) From (6) it follows that

$$(\psi_n, \phi)_{\mathbf{x}} = \mu_n a_n(t), \tag{8}$$

and

$$(a_n, \phi)_t = \mu_n \psi_n(x). \tag{9}$$

If we form the spatial and temporal correlation functions

$$K(\mathbf{x},\mathbf{y}) = (\phi(t,\mathbf{x}),\phi(t,\mathbf{y}))_t, \tag{10}$$

$$C(t,s) = (\phi(t,\mathbf{x}),\phi(s,\mathbf{x}))_{\mathbf{x}}, \tag{11}$$

then the back substitution of (8) into (9) yields

$$\sum_{\mathbf{y}} K(\mathbf{x},\mathbf{y})\psi(\mathbf{y}) = \mu^2\psi(\mathbf{x}), \tag{12}$$

which specifies ψ_n and ψ_m in (6), while (9) into (8) gives

$$\sum_{s} C(t,s)a(s) = \mu^2 a(t), \tag{13}$$

which specifies a_n and a_m in (5).

On general grounds, since the kernels K and C are symmetric, the existence of the decomposition, (7), has been demonstrated. The representation (7) can be referred to as the singular value decomposition (SVD) [18], (12) as the Karhunen-Lòeve (KL) procedure or principal components analysis [18] and (13) as the snapshot method [19]. From (8) and (9) it follows that only one of the two eigenfunction problems, (12), (13) need be solved. The basic method (but not in its statistical framework) is due to Schmidt [20]. (See [21] for further background.)

The two point correlation function, $K(\mathbf{x},\mathbf{y})$, measures the range of correlations present in the image data. The eigenfunctions of $K(\mathbf{x},\mathbf{y})$ can therefore be expected to isolate and rank coherent activity , i.e., to identify coherent structures. Patterns with chaotic appearance are seen in cortical images and are reminiscent of those seen in chaotic or turbulent fluid flows. The KL procedure has proven to be a highly successful means for treating the very complicated phenomena in such flows [22].

It is worth noting that the coordinates $\{a_n\}$ and $\{\psi_n\}$ are intrinsic to the data. As is well known, this coordinate system is optimal in the sense that the error incurred in any finite truncation of (7) is minimal over the class of orthogonal decompositions.

4 Filters

The response evoked by visual stimuli can be as small as $O(10^{-4})$ compared to the signal from the normal background activity at the cortical surface, and is

overwhelmed by other time-dependent activity engendered by respiration and pulse. A suite of procedures for eliminating unwanted signals have been developed in our laboratory [23]. These procedures, broadly referred to as indicator function methods, have the following features in common: 1) From records of unstimulated activity an image space, say B, is generated, which spans background and noise; 2) The projection operator, P_B, onto B is constructed from this; 3) Noise and background are removed by forming the indicator function $\tilde{\phi}$ for a given stimulus

$$\tilde{\phi} = \phi - P_B\phi \tag{14}$$

so that $(\tilde{\phi}, B) = 0$.

Here ϕ contains large spatial and temporal scales due to respiration and pulse, and also small spatial and temporal scales resulting from pixel noise, while in $\tilde{\phi}$, which may be regarded as a filtered version of ϕ, both large (respiration and pulse) and small scales (pixel noise) are removed. For the sake of simplicity we drop the tilde, and unless otherwise stated, in the following, ϕ refers to the filtered image or response.

5 Symmetries

For purposes of this exposition we restrict attention to the two visual modalities of ocularity and orientation. (As will be seen, directionality of motion is coupled to orientation and therefore will enter into the discussion.) The ocularity, $e(t)$, of a stimulus can take on the values r and ℓ for right and left eyes, respectively. In experiments, oriented stimuli are frequently drifting gratings composed of bars which are periodically repeated. Since these are of a stereotypical form it suffices to specify only their orientation, $\theta(t)$. Equation (4) above represents cortical images obtained in response to a stimulus $(e(t), \theta(t))$. (Recall that the focus is on average responses with transients averaged out in the analysis.)

The particular way in which ocularity and orientation are laid out on the visual cortex is not à priori known, nor is it important for our deliberations. The assumption which we make is that, irrespective of the ocular mapping, the layout is even-handed; that is, an extensive enough piece of tissue contains equal numbers of neurons devoted to the left and right eyes. For orientation, we assume that an oriented stimulus elicits a response from an equal number of neurons regardless of orientation. It is expected that, if a large enough piece of tissue is examined the principle of "even-handedness" will be respected in the statistics. As mentioned, the images have a chaotic-appearing character

and we will see that the eigenfunctions inherit this appearance. This does not conflict in any way with the notion of symmetry as used here. The symmetry lies in the mapping and not in the resulting pattern. The cortex creates a pattern according to a blueprint of its own. The principle of symmetry only requires that this plan treat right and left eyes equally and that all orientations be equally represented.

Symmetry, which can be marred by tissue size, may also be affected by noise. Another possible symmetry breaking is the "oblique effect", which suggests that orientation discrimination is stronger at vertical and horizontal orientations [24]. This small effect may be conditioned by environment, and would appear to differ from the slight ellipticity in orientation preference recently reported [25]. Effects of this sort, especially since they are small, can be treated by perturbation theory, from which it follows that subspaces are split and unperturbed eigenfunctions are distributed over several perturbed eigenfunctions. These small caveats withstanding, symmetry considerations have proven themselves to be a powerful tool for organizing and analyzing the data.

5.1 Ocularity

Here, as for orientation discussed below, the implications of even-handedness are probably more easily viewed in terms of the temporal correlation function. Since we have restricted attention to ocularity and orientation (11) takes the form

$$C = C(e(t),\ e(t'),\ \theta(t),\ \theta(t')) = C(e, e', \theta, \theta') \quad , \tag{15}$$

where the prime indicates another instant of time. C is a spatial average over the entire piece of tissue under investigation, which is assumed to be sufficiently large. Disregarding for the moment the role of orientation, the principle of even handedness therefore implies that $C(r, r) = C(\ell, \ell)$. In addition $C(r, \ell) = C(\ell, r)$ which follows directly from construction, (11). The correlation function is thus invariant under C_2, the cyclic group of two elements. This suggests that we can reduce the operators of (12) and (13) under the group representation of C_2. To accomplish this we write

$$\phi^{\pm}(\theta, \mathbf{x}) = \phi(r, \theta, \mathbf{x}) \pm \phi(\ell, \theta, \mathbf{x}) \tag{16}$$

and define

$$K^{\pm}(\mathbf{x}, y) = \sum_t \phi^{\pm}(t, \mathbf{x})\phi^{\pm}(t, \mathbf{y}). \tag{17}$$

A direct calculation then verifies that

$$K(\mathbf{x},\mathbf{y}) = \frac{1}{2}\left\{K^{+}(\mathbf{x},\mathbf{y}) + K^{-}(\mathbf{x},\mathbf{y})\right\} \tag{18}$$

The eigenfunctions of K^{+} and K^{-} are orthogonal. To verify this we observe that the snapshot method (Sirovich, 1987) states that the eigenfunctions of $K^{\pm}$, say $\psi^{\pm}$, are given by an admixture of the corresponding *snapshots*, *viz.,*

$$\psi^{\pm}(\mathbf{x}) = \sum_{t} \alpha^{\pm}(t)\phi^{\pm}(t,\mathbf{x}) \tag{19}$$

where the functions $\alpha^{\pm}(t)$ are to be determined. (These are in fact eigenfunctions of the corresponding $C^{\pm}(t,s)$ kernels.)

Substitution of (19) in $(\psi^{+},\psi^{-})_{\mathbf{x}}$ shows that this vanishes as a result of the already stated symmetry properties of $C(e,e')$.

5.2 Orientation

As part of the principle of even-handedness we assume that all orientations are equally represented. The second working assumption that we adopt is that the cross correlation, (11), satisfies

$$\begin{aligned} C(e,e',\theta,\theta') &= \sum_{\mathbf{x}} \phi(e,\theta,\mathbf{x})\phi(e',\theta',\mathbf{x}) \\ &= \sum_{\mathbf{x}} \phi(e,\theta+\theta_0,\mathbf{x})\phi(e',\theta'+\theta_0,\mathbf{x}) \\ &= C(e,e',\theta+\theta_0,\theta') \quad , \end{aligned} \tag{20}$$

for arbitrary θ_0. This simply says that if the two stimuli are rotated by the same amount, then the average across all pixels of the cross correlation remains unchanged. Aside from minor caveats stated above, this is a natural and reasonable assumption. It follows from this that the average over all pixels of the response product, (11), to two orientations only depends on the difference of these orientations, *viz.,*

$$C(e,e',\theta,\theta') = C(e,e',\theta-\theta') \tag{21}$$

If we assign the values $+1$ and -1 to the right and left eyes, then both symmetries can be incorporated into the statement that $C(e,e',\theta,\theta') = C(ee',\theta-\theta')$.

An immediate consequences of the form (21) is that the eigenfunctions of C are sinusoids in θ. It therefore follows from (19) that the spatial eigenfunctions are given by

$$\psi_n^{\pm}(\theta, \mathbf{x}) = \sum_{\theta} e^{in\theta} \phi^{\pm}(\theta, \mathbf{x}). \tag{22}$$

6 Eigenfunctions

We next discuss the form of the eigenfunctions obtained above and make comparisons with experimental results. In discussing the eigenfunctions, (22), it is useful to bear in mind that our images are represented by real numbers; this property is inherited by the correlation operator (15), which in turn must have real eigenfunctions as well. Thus, with the exception of $n = 0$, where only one eigenfunction emerges, the eigenfunctions come in pairs, the real and imaginary parts of (22), which pairwise decompose the space of images into invariant two-dimensional subspaces spanned by these image pairs. Here "invariance" has the following meaning. Let the cortical image, in response to a specific stimulus, be resolved as a superposition of these eigenfunctions. Then a geometrical rotation of the stimulus produces new superposition coefficients, which are obtained from the old by the simple action of two-dimensional orthogonal transformations within (and not between) those two-dimensional subspaces.

We first consider ψ_0^-, which from (22) is given by

$$\psi_0^- = \sum_{\theta} \{\phi(r, \theta, x) - \phi(\ell, \theta, x)\}. \tag{23}$$

This form which is the difference of right and left eye images corresponds to a traditional construction used in cortical imaging. As discussed in Section 4, background activity has been removed from ϕ. In an actual experiment, the image which is collected has the form $\phi_B + \phi(e, \theta, x)$, where ϕ_B is the portion of the image due to background. Thus the process of subtracting like images, (23), removes the background, and summation over all stimuli is equivalent to an ensemble average. The background is removed from the resulting construction and the two ocularities appear with different signatures. Figure 1 shows ocular dominance columns obtained by the subtraction procedure performed on cortical images from a macaque cortex. The result of of this experiment were unusual in that the picture shown in the figure almost identically coincides with one of the raw eigenfunctions, ψ, given by (12). In most instances noise intrudes and traces of ocular dominance columns can be seen in more than one raw eigenfunction. Filtering procedures, section 4, in particular indicator

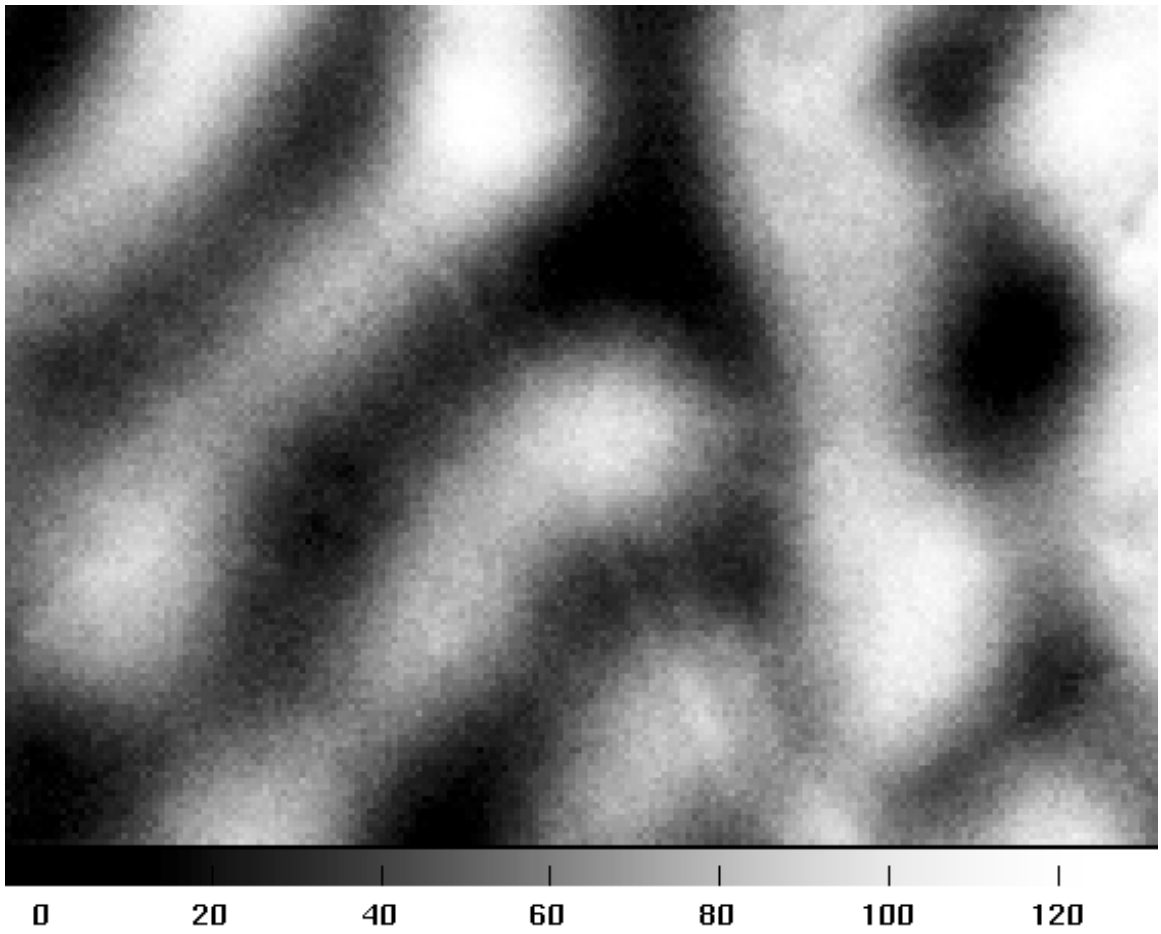

Fig. 1. Ocular dominance columns, found by subtraction, from a 4 mm × 3 mm patch of macaque striate cortex.

functions play a key role in extracting the latent information that is present in the data. This is illustrated in figure 2, which contrasts the refined eigenfunction $\psi_0^-(\mathbf{x})$, constructed from the indicator functions, with the subtraction picture. Clearly a far better image emerges from the refined eigenfunctions. It is worth mentioning that figure 2 shows data taken from cat cortex, where it is well-known that ocular dominance columns only appear faintly.

The images shown in figures 1 and 2 bring out activity correlated to ocularity, an architectural property. The structures exhibited in such figures are called ocular dominance columns, a term which derives from [4]. Thus we see that the symmetry implied by the even handedness principle furnishes a proof that the map of ocular dominance columns is an eigenfunction of the correlation operator $K(\mathbf{x}, \mathbf{y})$. The fact that one of the eigenfunctions is a well-known biological structure supports the suggestion that other eigenfunctions might also represent biologically-meaningful entities.

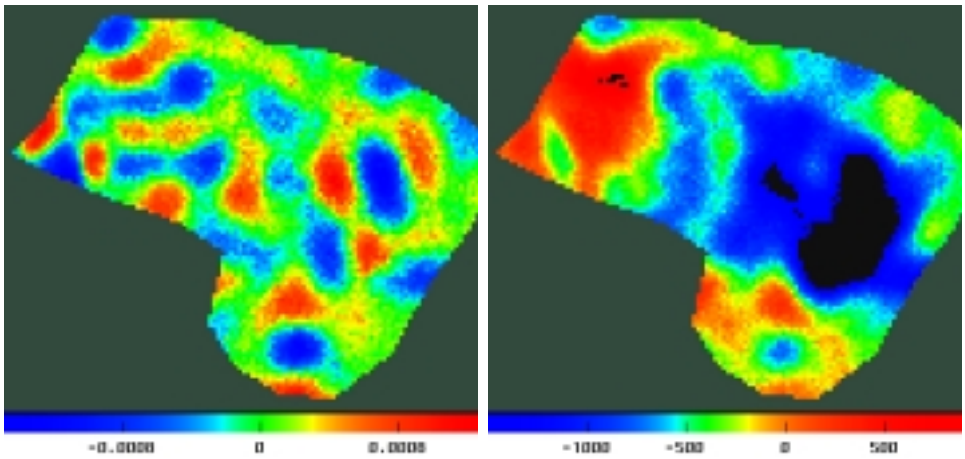

Fig. 2. **Left:** $\psi_0^-(\mathbf{x})$ describing ocular dominance columns found using indicator functions. (5mm $\times$ 5mm patch of area 17 of cat striate cortex.) **Right:** Subtraction picture of the same data. The color scale for the subtraction picture has been adjusted to emphasize the similarity between the bottom "toe" regions of the two pictures.

Next we consider ψ_0^+, which from (22) is given by

$$\psi_0^+ = \sum_\theta (\phi(r, \theta, \mathbf{x}) + \phi(\ell, \theta, \mathbf{x})). \tag{24}$$

Clearly this furnishes a response map of the cortex due to the summed activity due to both eyes. Unlike ψ_0^- there is no like image produced in traditional laboratory practice, since background effects are overwhelmingly large compared to the signal and straightforward procedures, like subtraction of the mean image, are not adequate for the removal of the background. Since experimental confirmation of this modality is not yet available we do not dwell further on this result.

As a next case we consider

$$\psi_1^+ = \sum_{0 \le \theta \le 2\pi} e^{i\theta} \phi^+(\theta, \mathbf{x}). \tag{25}$$

To gain insight into the meaning of this eigenfunction, we rewrite the summation as

$$\psi_1^+ = \sum_{0 \le \theta \le \pi} e^{i\theta} \{\phi^+(\theta, \mathbf{x}) - \phi^+(\theta + \pi, \mathbf{x})\}. \tag{26}$$

A neuron (or a pixel location) which responds purely to orientation does so equally for θ and $\theta + \pi$ and in such a case the summand in (25) vanishes. Single electrode recordings confirm the existence of such neurons [26]. Electrode

recording also confirms the presence of directional neurons, *i.e.,* neurons which respond to gratings drifting in the direction θ, but not at all to gratings drifting in the direction $\theta + \pi$. Clearly such neurons code for motion directionality, and it is only such neurons that contribute to the summation in (25). Thus ψ_1^+ yields a map of the distribution of directionally sensitive neurons.

The second harmonic,

$$\psi_2^+ = \sum_{0 \le \theta < 2\pi} e^{i2\theta} \phi^+(\theta, \mathbf{x}), \tag{27}$$

can be written as

$$\psi_2^+ = \sum_{0 \le \theta < \pi} e^{i2\theta} \{\phi^+(\theta, \mathbf{x}) + \phi^+(\theta + \pi, \mathbf{x})\}. \tag{28}$$

For neurons which code for orientation $\phi^+(\theta, \mathbf{x}) = \phi^+(\theta + \pi, \mathbf{x})$, while for neurons which code for directionality only one term of the sum can be non-zero. Thus the eigenfunction ψ_2^+, carries both orientational and directional information, in contrast to ψ_1^+ which is purely directional. ψ_2^+ provides us with a map of neuronal sites which respond to orientation and subserves purely directional sites.

In figures 3 and 4 we show ψ_1^+ and ψ_2^+, which are conveniently represented by amplitude and phase maps. An interesting feature of both figures is the presence of *pinwheels* in the phase maps. Each pinwheel includes a singular point where zones of differing constant phase meet, and of necessity must correspond to a locus of zero amplitude. Indeed, this is the only means by which a complex number may vary smoothly and yet undergo a half cycle phase change. Bonhoeffer [27] and Blasdel [8] by using subtraction methods to eliminate background, first produced orientation preference maps. These furnish loci of maximal response to oriented stimuli. Generally, directional effects are small compared to orientation effects, and as a result the phase map of ψ_2^+ lies close to the orientation preference maps. This, therefore, is a second instance for which we can demonstrate that a single eigenfunction of $K(\mathbf{x}, \mathbf{y})$ can be identified with an already known experimental structure.

Other modalities, such as ψ_1^- and ψ_2^-, still need experimental verification and will be discussed elsewhere.

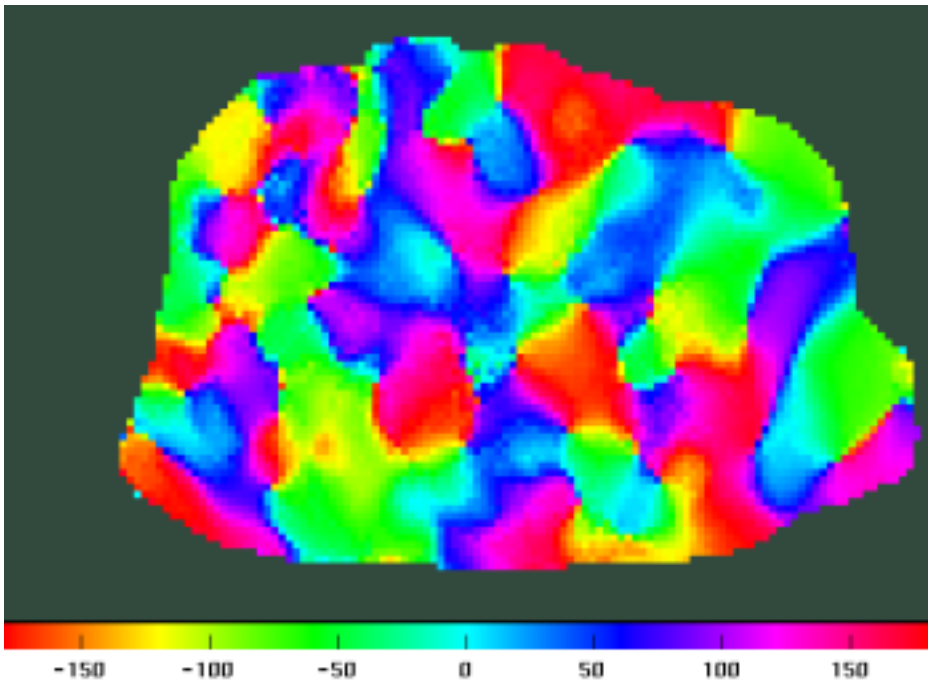

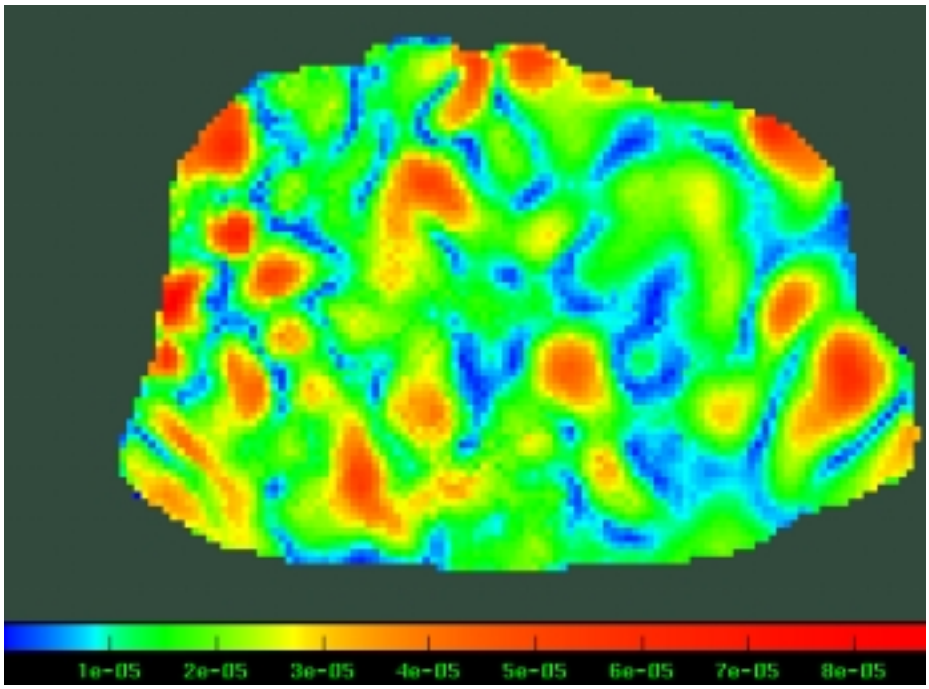

Fig. 3. The function $\psi_1^+(\mathbf{x})$, describing the directional response from area 17/18 in the cat. The function is shown as a phase and an amplitude: the phase gives the direction to which cells at $\mathbf{x}$ are tuned and the amplitude gives the magnitude of the response.

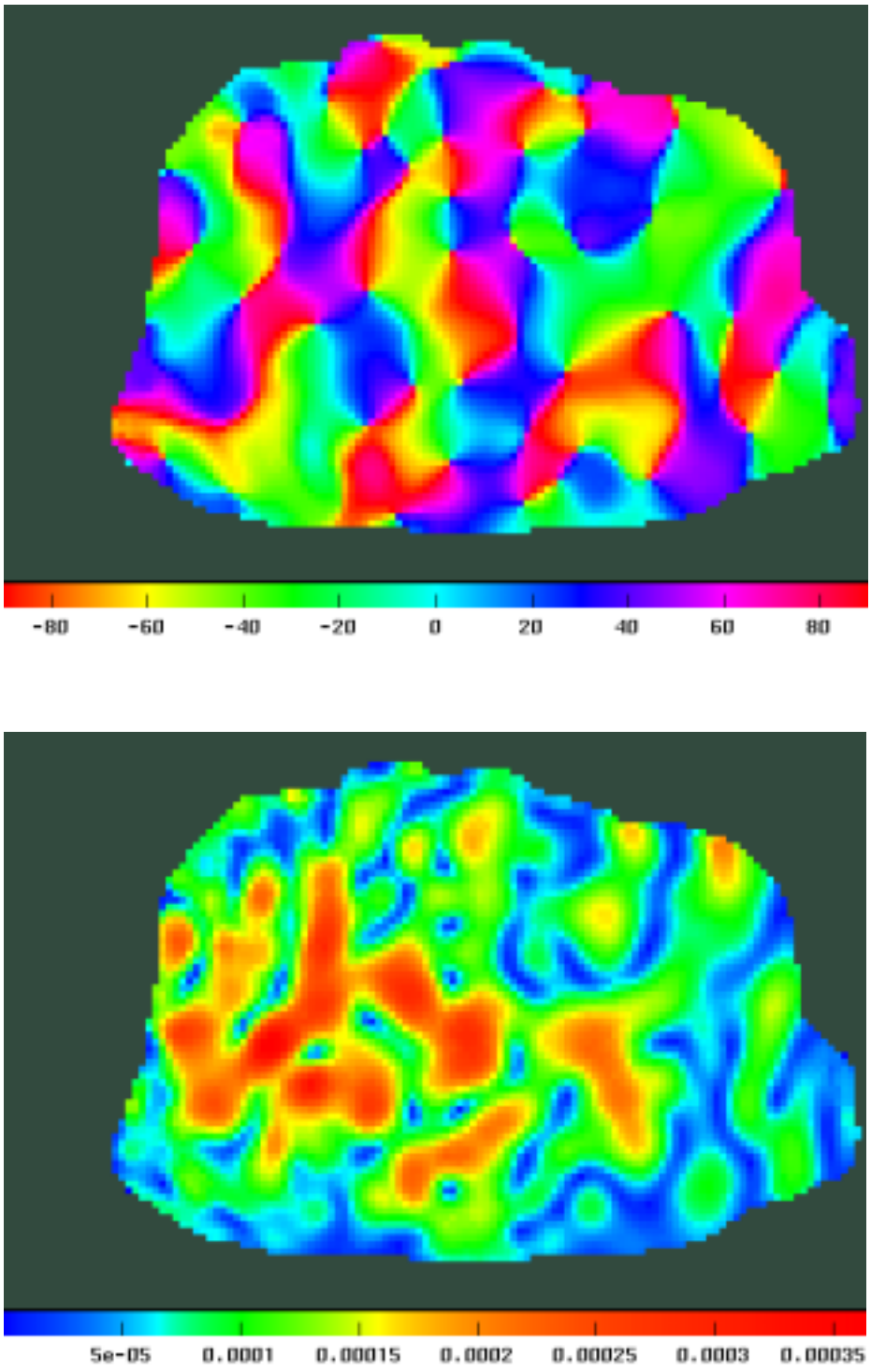

Fig. 4. The function $\psi_2^+(\mathbf{x})$, describing the orientation response from area 17/18 in the cat. The function is shown as a phase and an amplitude: the phase gives the orientation to which cells at $\mathbf{x}$ are tuned and the amplitude gives the magnitude of the response.

7 Dimension Considerations

Although the nature and character of dynamical systems which might describe cortical dynamics has not been discussed, the structures which would emerge from such a dynamical formulation are revealed by this analysis. Moreover, we are in a position to make some educated speculations on what might be the number of dynamical variables needed to describe such a dynamical system.

In our experiments the tissue sizes are typically 35 mm^2. For these experiments, the analysis indicates that 30 eigenfunctions appear to overestimate the number of active modes. In as much as dimension is an extensive measure, 10^2 modes/cm^2 appears to be a safe estimate and from this 1.5×10^3 modes would appear to be a fair estimate of the modes needed to account for activity in a cortex covering 15 cm^2. However, this estimate does not take into account all the modalities of the visual cortex, nor have all the scales been fully explored. Additionally parametric changes in the structures of the response due to wavenumber and frequency variation in the stimulus will require further study.

This problem of dimension may also be addressed in a different, but related manner. All visual modalities must find representation in the cortex, and this must be true for every position of visual space. Results from single cell recordings and staining methods reveal that, although not strictly periodic, the architecture of the primary visual cortex is repetitive. This is evidenced in at least two ways: (1) By the presence of ocular dominance columns, each of which has a width of roughly 500μm and which appear as relatively irregular stripes; (2) By the presence of "cytochrome oxidase blobs", patches where a metabolic enzyme appears in increased concentration and where there is a rich blood supply to the cortex [28]. These are also roughly 500μm from one another. The prevailing (although controversial) view is that the blobs mediate color vision. Ts'o and Gilbert [29] have further suggested that two sorts of blobs are required to account for the two opponent mechanisms of color vision. On this basis a full complement of modalities is spread over approximately 1 mm^2. Thus in this picture visual space is sampled by approximately 1500 sampling regions. (This compartmentalized view is easily replaced by a continuously varying model.) The question of how many mathematical modes are needed for a full complement of visual modalities is difficult to answer. If we take 10 as a nominal estimate then a model incorporating 15,000 modes would be necessary to simulate the primary visual cortex, which is an order of magnitude larger than the above rough and incomplete estimates in which just 1 mode/mm^2 was obtained.

Both lines of argument given above lack the precision we would like to achieve in a discussion of this sort. At best the estimates are nominal. However, the

main thrust of the argument is that $O(10^4)$ appears to be a reasonable count on the number of modes at work in the primary visual cortex. In comparison with the $O(10^8)$ neurons present, this represents a vast compression, and implies that, due to correlations in the activities of individual neurons, a great redundancy is suggested in a naive count which estimates the number of separate variables by the numbers of neurons in the cortex.

8 Concluding Remarks

We have made use of the KL procedure as a broad framework for developing tools for examining and analyzing image data obtained from the mammalian visual cortex. This procedure furnishes the tools for filtering out background (vegetative) activity, artifacts and noise from the signal. We are then left with the response to the visual stimulation, a signal which can be as small as $O(10^{-4})$ of the recorded signal in the optical image.

The data can be further refined by means of two symmetry principles, each based on reasonable hypotheses. A result of this was the demonstration that ocular dominance maps are eigenfunctions of the correlation operator. It was also demonstrated that other eigenfunctions carry orientational and directional information. In the absence of their experimental confirmation, we have not discussed the biological relevance of the other eigenfunctions that emerge as a consequence of the analysis. It is worth mentioning that other modalities also can be treated within the theoretical framework presented here. For example, color opponency should be amenable to the same simple group theory analysis as was used in the case of ocularity.

We end on a note of caution. It should be noted that images of small, bounded samples of real neural tissue can be expected to depart from the ideal used in the analysis, not strictly obeying the symmetry principles. For example, if the tissue is not sufficiently large then we fall short of achieving symmetry due to unequal populations of neurons. (A piece of tissue containing just one ocular dominance column obviously destroys the right-eye/left-eye symmetry.) Nevertheless the organizing principles which follow from the symmetry analysis have proved itself capable of extracting meaningful structures from noisy data where other methods fail.

Acknowledgement

This work was supported by grants from the Office of Naval Research (N00014-95-1-0281 & N00014-93-1-0279) and the National Institutes for Mental Health (R01MH50166-01).

References

[1] B. Katz. The nerve impulse. *Sci. Am.*, 187:55–64, 1952.

[2] F. Worgotter and C. Koch. A detailed model of the primary visual pathway in the cat: Comparison of afferent excitatory and intracortical inhibitory connection schemes for orientation selectivity. *J. Neuroscience*, 11:1959–1979, 1991.

[3] M. N. Chee-Orts, K.P. Purpura, and L.M. Optican. A dynamical model of the primate's early visual pathway: Effect of luminance contrast, spatial scale, and spatial orientation in shaping neuronal firing patterns. 1995. *(in preparation).*

[4] D.H. Hubel and T.N. Wiesel. Receptive fields, binocular interaction and functional architecture in the cat's visual cortex. *J. Physiol. (Lond)*, 160:106–154, 1962.

[5] D.H. Hubel and T.N. Wiesel. Sequence regularity and geometry of orientation columns in the monkey striate cortex. *J.Comp.Neurol.*, 158:267–294, 1974.

[6] S. LeVay and S.B. Nelson. Columnar organization of the visual cortex. In A.G. Leventhal, editor, *Vision and Visual Dysfunction (The Neural Basis of Visual Function)*, pages 266–3l5. Macmillan Press, 1991.

[7] G.G. Blasdel. Differential imaging of ocular dominance and orientation selectivity in monkey striate cortex. *J. Neuroscience*, 12:3115–3138, 1992.

[8] G.G. Blasdel. Orientation selectivity, preference, and continuity in monkey striate cortex. *J. Neuroscience*, 12:3139–3161, 1992.

[9] G.G. Blasdel and G. Salama. Voltage-sensitive dyes reveal a modular organization in monkey striate cortex. *Nature*, 321:579–585, 1986.

[10] A. Grinvald, E. Lieke, R.D. Frostig, C.D. Gilbert, and T.N. Wiesel. Functional architecture of cortex revealed by optical imaging of intrinsic signals. *Nature*, 324:361–364, 1986.

[11] D.Y. Ts'o, R.D. Frostig, E.E. Lieke, and A. Grinvald. Functional organization of primate visual cortex revealed by high resolution optical imaging. *Science*, 249:417–420, 1990.

[12] D.H. Hubel and T.N. Wiesel. Functional architecture of macaque monkey visual cortex. *Proc. Roy. Soc. Lond. B*, 198(1-59), 1977.

[13] V. Braitenberg and C. Braitenberg. Geometry of orientation columns in the visual cortex. *Biol.Cybern.*, 33:179–186, 1979.

[14] K.G. Gotz. Do "d-blob" and "l-blob" hypercolumns tessellate the monkey visual cortex? *Biol.Cybern.*, 56:107–109, 1987.

[15] E. Erwin, K. Obermayer, and K. Schulten. Models of orientation and ocular dominance columns in the visual cortex: A critical comparison. *Neur.Comp.*, 7:425–468, 1995.

[16] L.B. Cohen, H.V. Davila, D. Landowne, A.S. Wagonner, and C.H. Wang. Changes in axon fluorescence during activity: molecular probes of membrane potential. *J. Membr. Biol.*, 19:1–36, 1974.

[17] E.E Lieke, R.D. Frostig, A. Arieli, D.Y. Ts'o, R. Hildesheim, and A. Grinvald. Optical imaging of cortical activity: Real-time imaging using extrinsic dye-signals and high resolution imaging based on slow intrinsic-signals. *Annu. Rev. Physiol.*, 51:543–559, 1989.

[18] G.W. Stewart. On the early history of the singular value decomposition. *SIAM Review*, 35(4):551–566, 1993.

[19] L. Sirovich. Turbulence and the dynamics of coherent structures, pt i: Coherent structures, pt ii: Symmetries and transformations, pt. iii: Dynamics and scaling. *Quarterly of Applied Mathematics*, XLV(3):561–590, 1987.

[20] E. Schmidt. Zur Theorie Der Linearen Und Nichtlinearen Integralgleichungen. I Teil: Entwicklung WillküLicher Funktion Nach Systemen Vorgeschriebener. *Mathenatische Annalen*, 63:433–476, 1907.

[21] L. Sirovich and R.M. Everson. Analysis and management of large scientific databases. *International Journal of Supercomputing Applications*, 6(1):50–68, 1992.

[22] L. Sirovich. Chaotic dynamics of coherent structures. *Physica*, 37D:126–145, 1989.

[23] R.M. Everson, L. Sirovich, B.W. Knight, E. Kaplan, E. O'Brien, and D. Orbach. Optical imaging of the mammalian visual cortex. *Bio. Bull.*, 1995. *(submitted).*

[24] D.H. Foster. Operating on spatial relations. In R.J. Watt, editor, *Pattern recognition by man and machine*, volume 14 of *Vision and visual dysfunction*, chapter 50-68. Macmillan Press, 1991.

[25] K. Obermayer and G.G. Blasdel. Geometry of orientation and ocular dominance colums in monkey striate cortex. *J. Neuroscience*, 13(10):4114–4129, 1993.

[26] D.H. Hubel and T.N. Wiesel. Cells sensitive to binocular depth in area 18 of the macaque monkey ccortex. *Nature*, 225:41–42, 1970.

[27] T. Bonhoeffer and A. Grinvald. Iso-orientation domains in cat visual cortex are arranged in pinwheel-like patterns. *Nature*, 353:429–431, 1991.

[28] M.T.T. Wong-Riley. Changes in the visual system of monocularly sutured or enucleated cats demonstrable with cytochrome oxidase histochemistry. *Br.Res.*, 17:11–28, 1979.

[29] D.Y. Ts'o and C.D. Gilbert. The organization of chromatic and spatial interactions in the primate striate cortex. *J.Neurosc.*, 8:1712–1727, 1988.